European Journal of Medicinal Chemistry 226 (2021) 113827

Contents lists available at ScienceDirect

European Journal of Medicinal Chemistry

journal homepage: http://www.elsevier.com/locate/ejmech

A tacrine-tetrahydroquinoline heterodimer potently inhibits acetylcholinesterase activity and enhances neurotransmission in mice

Fanny C.F. Ip [a, b, c, 1], Guangmiao Fu [a, 1], Fengzhi Yang [d], Fangyuan Kang [a], Peiran Sun [a], Choi Ying Ling [a], Kit Cheung [a], Fangzhou Xie [d], Yueqing Hu [a], Lei Fu [d, *], Nancy Y. Ip [a, b, c, **]

[a] Division of Life Science, State Key Laboratory of Molecular Neuroscience and Molecular Neuroscience Center, The Hong Kong University of Science and Technology, Clear Water Bay, Kowloon, Hong Kong, China
[b] Hong Kong Center for Neurodegenerative Diseases, Hong Kong Science Park, Hong Kong, China
[c] Guangdong Provincial Key Laboratory of Brain Science, Disease and Drug Development, Shenzhen–Hong Kong Institute of Brain Science, HKUST Shenzhen Research Institute, Shenzhen, Guangdong, 518057, China
[d] School of Pharmacy, Shanghai Jiao Tong University, Shanghai, China

ARTICLE INFO

Article history:
Received 25 May 2021
Received in revised form
26 August 2021
Accepted 2 September 2021
Available online xxx

Keywords:
Cognitive function
Dementia
Electrophysiological recordings
Hybrid
Synaptic plasticity

ABSTRACT

Cholinergic neurons are ubiquitous and involved in various higher brain functions including learning and memory. Patients with Alzheimer's disease exhibit significant dysfunction and loss of cholinergic neurons. Meanwhile, such cholinergic deficits can be potentially relieved pharmacologically by increasing acetylcholine. Acetylcholinesterase (AChE) inhibitors have been used to improve cholinergic transmission in the brain for two decades and have proven effective for alleviating symptoms in the early stages of Alzheimer's disease. Therefore, the search for AChE inhibitors for drug development is ongoing. The enzymatic pocket of AChE has long been the target of several drug designs over the last two decades. The peripheral and catalytic sites of AChE are simultaneously bound by several dimeric molecules, enabling more-efficient inhibition. Here, we used 6-chlorotacrine and the tetrahydroquinolone moiety of huperzine A to design and synthesize a series of heterodimers that inhibit AChE at nanomolar potency. Specifically, compound **7b** inhibits AChE with an IC_{50} < 1 nM and spares butyrylcholinesterase. Administration of **7b** to mouse brain slices restores synaptic activity impaired by pirenzepine, a muscarinic M1-selective antagonist. Moreover, oral administration of **7b** to C57BL/6 mice enhances hippocampal long-term potentiation in a dose-dependent manner and is detectable in the brain tissue. All these data supported that **7b** is a potential cognitive enhancer and is worth for further exploration.

1. Introduction

Cholinergic neurons, which utilize acetylcholine as a neurotransmitter, are ubiquitous and involved in various higher brain functions including learning and memory [1]. They project to the cortex and hippocampus, and primarily originate from the basal forebrain. Patients in the early and late stages of Alzheimer's disease exhibit significant dysfunction and loss of cholinergic neurons in the basal forebrain, respectively [2]. Such cholinergic deficits can be potentially relieved pharmacologically by increasing acetylcholine or *via* agonistic activation of acetylcholine receptor at postsynaptic sites [3–5]. Three of the four US FDA-approved drugs, *i.e.*, donepezil, galantamine, and rivastigmine, as well as huperzine A (approved by China NMPA) are acetylcholinesterase (AChE: EC 3.1.1.7) inhibitors that increase acetylcholine levels at synapses and enhance neurotransmission. Although they only provide symptomatic relief, AChE inhibitors remain first-line treatments for cognitive impairment, Alzheimer's disease, and Parkinson's disease [6]. Thus, the search for AChE inhibitors for drug development is ongoing [7–9].

The enzymatic pocket of AChE is a distinct and well-studied structure that is being targeted for the design of new inhibitors [10]. The peripheral and catalytic sites of AChE are located in 2 spatial regions. Accordingly, several hybrid and dimeric molecules have been designed to simultaneously bind these sites to exert their effects more efficiently [11]. Strategies to include the active

* Corresponding author.
** Corresponding author. Division of Life Science, The Hong Kong University of Science and Technology, Clear Water Bay, Hong Kong, China.
E-mail addresses: leifu@sjtu.edu.cn (L. Fu), boip@ust.hk (N.Y. Ip).
[1] These authors contributed equally.

https://doi.org/10.1016/j.ejmech.2021.113827
0223-5234/

Abbreviations

AChE	acetylcholinesterase
BChE	butyrylcholinesterase
LTP	long-term potentiation
fEPSP	field excitatory postsynaptic potential
P_{adj}	adjusted *P* value
FPKM	fragments per kilobase of exon model per million reads mapped
GO	Gene Ontology
IEGs	immediate early genes

scaffolds of existing Alzheimer's disease drugs, such as tacrine, donepezil, and huperzine A, as well as antioxidants and flavonoids have been employed for this purpose [12–16]. Thus, utilizing this dimerization strategy is expected to increase the potency and specificity of AChE inhibitors [17].

Given this context, in this study, we designed and synthesized a series of heterodimers using 6-chlorotacrine and the tetrahydroquinolone moiety of huperzine A. Among these heterodimers, compound **7b** significantly inhibits AChE activity at nanomolar concentrations. Moreover, it exhibits higher selectivity for AChE over butyrylcholinesterase (BChE), a cholinesterase mainly found in blood plasma. Furthermore, pilot toxicity and pharmacokinetic analyses show that after oral administration, **7b** enters the systemic circulation and can penetrate the blood–brain barrier. Finally, in mice, **7b** administration enhances synaptic activity in the form of long-term potentiation (LTP) under physiological stimulation and prevents the LTP impairment induced by an M1 receptor antagonist *in vitro*. All these data supported the notion that **7b** is a potential cognitive enhancer and is worth for further exploration.

2. Results and discussion

2.1. Synthesis of heterodimers 7a–7i

A series of heterodimers comprising 6-chlorotacrine and 1,5,7,8-tetrahydroquinoline-2,6-dione (**3**) connected through an aminoalkane linker were synthesized. The number of methylenes in the linker was increased systematically to determine the optimal length for maximal AChE inhibition. The general synthesis for heterodimers **7a**–**7i** is shown in Scheme 1. The details of synthesis and chemical characterization are described in section *4.2. Chemistry*. Condensation–cyclization of commercially available 1,4-cyclohexanedione mono-ethylene ketal (**1**) with methyl propiolate under a 7-N ammonia solution in methanol in a sealed tube yielded 1,5,7,8-tetrahydro-quinoline-2,6-dione 6-ethylene glycol ketal (**2**) [18]. The carbonyl-protecting group of **2** was deprotected in a solution of *p*-toluenesulfonic acid, yielding **3** [19]. Next, 6,9-dichloro-1,2,3,4-tetrahydroacridine (**5**) was prepared from commercially available 4-chloroanthranilic acid (**4**) as previously reported [20]. The 9-chloro of **5** was substituted with appropriate 1,ω-diaminoalkanes to yield the desired intermediates *N*-(6-chloro-1,2,3,4-tetrahydroacridin-9-yl)alkane-1,ω-diamines (**6a**–**6i**) [21,22]. The spectral data were concordant with the literature [20]. The analytical, NMR spectra and data, and mass spectral data of intermediates **2, 3, 5** and **6a-6i** were concordant with their respective structures (*Supplementary Information S1 and S2*). Finally, the intermediates with different linker sizes (**6a**–**6i**) were coupled to **3** in the presence of dichloromethane and sodium triacetoxyborohydride under the catalysis of acetic acid to afford heterodimers **7a**–**7i** at a moderate yield (34–43%). Structural determination and signal assignment of the final compounds were accomplished by NMR analysis including ^{1}H NMR and ^{13}C NMR as well as high-resolution mass spectrometry (*Supplementary Information S2*).

2.2. Effects of heterodimers on cholinesterase inhibition, HepG2 cell viability, and hERG channel activity

AChE promotes amyloid-beta fibril formation, whereas BChE prevents this and delays the formation of amyloid-beta aggregation in the brain [23,24]. Therefore, an inhibitor with greater selectivity for AChE over BChE is preferable for the treatment of Alzheimer's disease. The *in vitro* AChE and BChE activities of all synthesized compounds **7a**–**i** were evaluated using Ellman's method and compared to those of donepezil and tacrine (Fig. 1a). All 9 synthesized heterodimeric compounds exhibited a dose-dependent inhibitory effect on AChE (Fig. 1a); 4 of them exhibited an IC_{50} < 10 nM (Table 1). Among them, compound **7b** (with a methylene linker $n = 3$) was the most potent, with an IC_{50} of 0.9 ± 0.06 nM, making it 200 times more potent than tacrine (IC_{50} = 237 ± 15 nM) (Fig. 1a, Table 1). Except **7a**, when the number of methylenes in the linker increases, the compound's potency to inhibit AChE decreases accordingly. All compounds selectively inhibited AChE as indicated by the ratio of the average IC_{50} of BChE to that of AChE (range: 23–222, Table 1).

The mode of the inhibitory mechanism of 7b on AChE was subsequently examined. AChE activity was measured in the presence of 4 different concentrations of 7b (*i.e.*, 0, 0.5, 1.0, or 1.5 nM) or tacrine as a control (*i.e.*, 0, 75, 150, or 225 nM), with a substrate concentration ranging from 0.16 to 1.00 mM. Lineweaver–Burk plots showed that all linear-fitted equations intersected the left quadrant for 7b, indicating that it is a mixed-type inhibitor (Fig. 1b) similar to tacrine [25].

The *in vitro* cytotoxic effect of 7b was assessed using the HepG2 human liver cell line and a Chinese hamster ovary cell line expressing hERG (a potassium ion channel). Accordingly, 7b exhibited a cytotoxic effect similar to tacrine. The IC_{50} values for 7b and tacrine in HepG2 cells were 11 and 14 μM, respectively (Table 2). The IC_{50} values of 7b and tacrine on hERG channel activity were 9 and 14 μM, respectively. Compared to the IC_{50} values of 7b on HepG2 and hERG to that on AChE, 7b exhibited a relatively larger treatment window. The ratios of the liver toxicity of 7b and tacrine were 119162 and 611, respectively (Table 2). Similarly, the ratios of the cardiac toxicity of 7b and tacrine were 9972 and 60, respectively (Table 2). These results collectively indicate that 7b is the best compound within this series of heterodimeric compounds in terms of potency and selectivity.

2.3. Molecular modeling of the interaction between 7b and AChE

Given the mixed-type inhibitory nature of 7b, its interaction with the active site of AChE was subsequently investigated. AChE has a characteristic 20 Å-deep gorge whose bottom harbors the active site, which includes the catalytic triad and several substrate-binding pockets including the catalytic anionic site that binds to the choline moiety [10]. The entrance of the gorge has a peripheral anionic site that the substrate binds transiently. Some AChE inhibitors such as tacrine, galantamine, and huperzine A bind solely to the active site, whereas others such as donepezil also bind to the peripheral anionic site [26]. It was reasoned that linking the 6-chlorotacrine and tetrahydroquinolone moieties would enable the heterodimers to bind to both the catalytic and peripheral anionic sites, thus increasing binding affinity to AChE. Accordingly, computational docking studies were performed to model the association between 7b and AChE (its substrate) at the target-binding

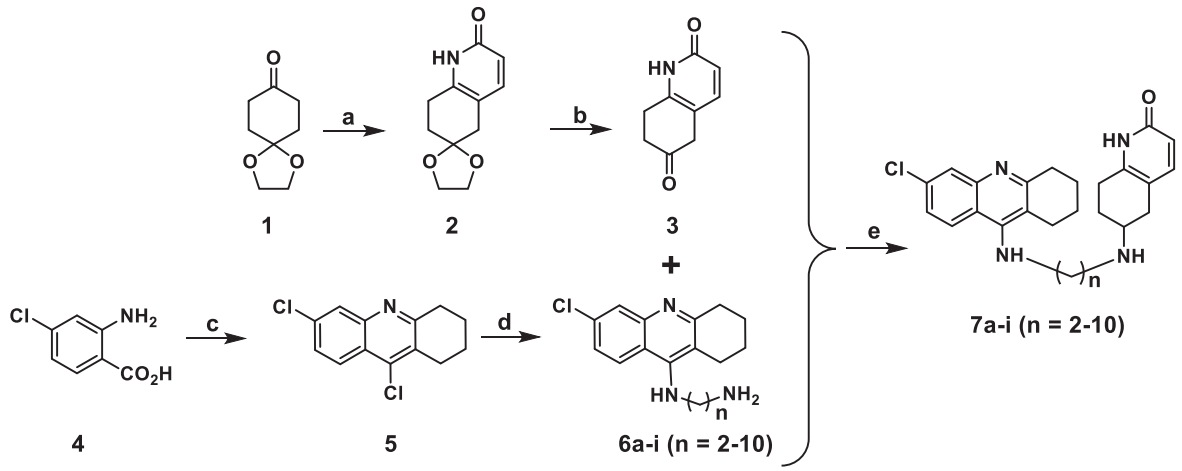

Scheme 1. Synthesis of a series of tacrine-tetrahydroquinolone heterodimers. Reagents and conditions: (a) methyl propiolate, 7 N NH_3/MeOH, 120 °C, 24 h; (b) *p*-toluenesulfonic acid, water, 100 °C, 3 h; (c) cyclohexanone, $POCl_3$, 120 °C, 8 h; (d) diaminoalkanes, 1-pentanol, 160 °C, 48 h; (e) $NaB(OAc)_3H$, cat. AcOH, dichloromethane.

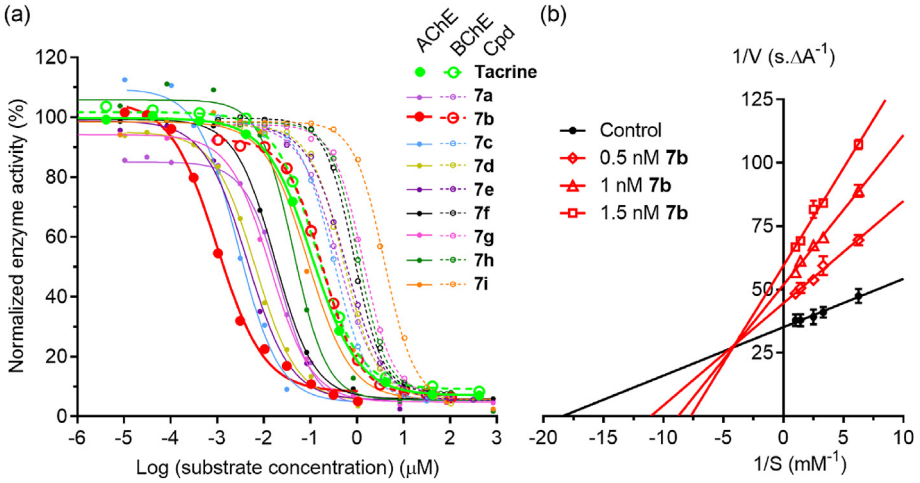

Fig. 1. (a) Dose–response curves of the cholinesterase inhibitory activities of heterodimers. Representative concentration–responses of the hybrid compounds and tacrine in acetylcholinesterase (AChE) and butyrylcholinesterase (BChE) assays. The data were fitted using the Hill equation, and IC_{50} values are shown (AChE; BChE). Tacrine (bright green) and 7b (red) are highlighted as larger symbols, and bold and dotted lines depict AChE and BChE, respectively. (b) Study of the enzyme inhibition mechanism of 7b. Lineweaver–Burk plots of the inhibition of AChE by 7b, indicating that 7b is a mixed-type inhibitor.

Table 1
Inhibitory effects of heterodimers on AChE and BChE enzyme activities.

Compound	MW	cLogP	Length of linker	IC_{50} on AChE (nM)			IC_{50} on BChE (nM)			Specificity ratio[a]
Donepezil	379	4.6	–	42.82	±	9.72	12773	±	915	298
Tacrine	198	3.27	–	237	±	15	147	±	11	0.6
7a	423	4.32	2	17.7	±	2.98	401	±	4	23
7b	437	4.66	3	0.9	±	0.06	200	±	16	222
7c	451	4.55	4	2.94	±	0.65	347	±	15	118
7d	465	5.08	5	5.66	±	0.94	503	±	9	89
7e	479	5.61	6	6.02	±	2.1	574	±	26	95
7f	493	6.14	7	14.78	±	2.92	893	±	45	60
7g	507	6.67	8	12.74	±	2.95	1364	±	22	107
7h	521	7.2	9	29.06	±	7.92	1075	±	11	37
7i	535	7.73	10	66.05	±	10.96	3779	±	46	57

Values are expressed as the mean ± standard deviation of at least 3 independent experiments.
AChE: acetylcholinesterase; BChE: butyrylcholinesterase; MW: molecular weight; cLogP: calculated octanol/water partition coefficient.
[a] The specificity ratio is defined as the IC_{50} of BChE inhibition divided by the IC_{50} of AChE inhibition: larger ratios indicate greater specificity of the compound towards AChE inhibition over BChE inhibition.

site in AChE (Fig. 2). Docking studies revealed that in its *R*-isomer conformation, 7b binds to both the catalytic and peripheral anionic sites of AChE. Furthermore, there was an unusual mode of binding at the Trp286 residue of AChE, wherein apart from a hydrogen bond between Trp286 and the amide-NH within the tetrahydroquinolone moiety of 7b, Trp286 was flipped, forming a hydrophobic interaction with the tetrahydroquinolone moiety (Fig. 2).

Table 2
Inhibitory effects of the heterodimers on HepG2 viability and hERG channel activity.

Compound	IC_{50} on HepG2 viability (nM)			Liver toxicity ratio[a]	IC_{50} on hERG activity (nM)			Cardiac toxicity ratio[b]
Donepezil	262727	±	35797	6136	8718	±	1643	204
Tacrine	144826	±	9218	611	14312	±	4707	60
7a	213994	±	35673	12090	2408	±	421	136
7b	107246	±	8907	119162	8975	±	827	9972
7c	110203	±	20674	37484	8069	±	1203	2745
7d	47187	±	5269	8337	7657	±	993	1353
7e	51310	±	7663	8523	11637	±	899	1933
7f	39247	±	5359	2655	6357	±	195	430
7g	42583	±	9930	3342	2191	±	196	172
7h	35546	±	6611	1223	2755	±	342	95
7i	17189	±	3561	260	2768	±	238	42

Values are expressed as the mean ± standard deviation of at least 3 independent experiments.
[a] The liver toxicity ratio is defined as the IC_{50} of HepG2 cytotoxicity divided by the IC_{50} of AChE inhibition: larger ratios indicate lower toxicity of the compound to HepG2 liver cells.
[b] The cardiac toxicity ratio is defined as the IC_{50} of hERG channel inhibition divided by the IC_{50} of AChE inhibition: larger ratios indicate lower toxicity of the compound on cardiac cells.

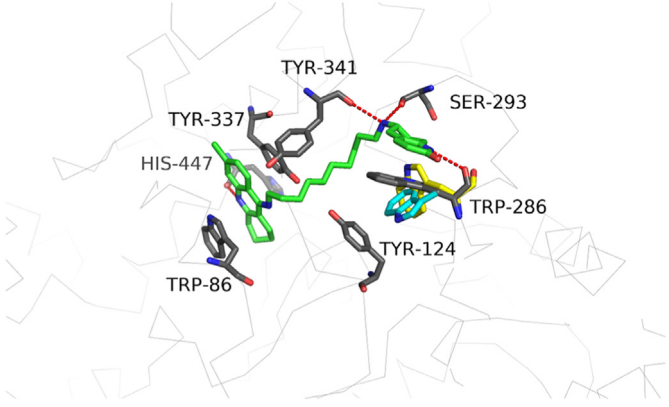

Fig. 2. Conformation of (*R*)-7b docked into acetylcholinesterase (AChE); 7b is depicted as green sticks. Grey ribbons and sticks indicate the conformation of AChE after docking. Red dashed lines represent hydrogen bonds. The conformation of Trp286 before docking is shown as yellow sticks, and the conformation of the corresponding Trp279 in *Tetronarce californica* AChE-bis(7)-tacrine complex (PDB ID: 2CKM) is shown as cyan sticks.

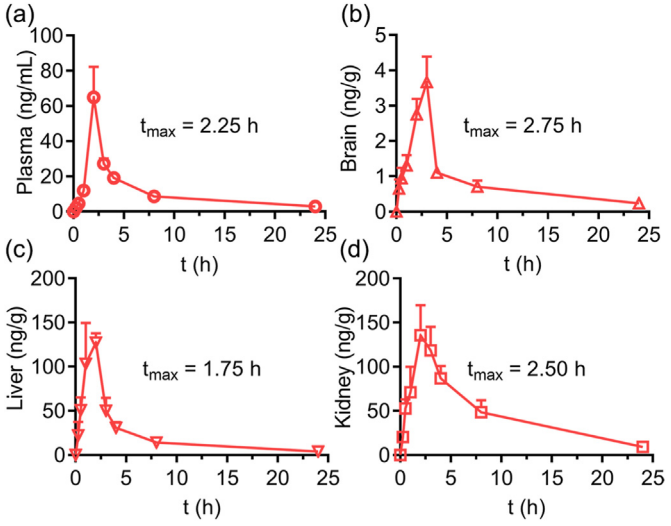

Fig. 3. *In vivo* pharmacokinetics of 7b. C57BL/6 mice were orally administered 7b at 10 mg/kg. The concentrations of 7b in (a) plasma, (b) the brain, (c) liver and (d) kidney were detected by UPLC-mass spectrometry. The time to reach maximum concentration (t_{max}) in each tissue is shown.

2.4. In vivo pharmacokinetic study and in vitro physicochemical properties of 7b

To investigate the blood–brain barrier permeability of 7b, its pharmacokinetics was investigated in various body organs/tissues in mice after oral administration at 10 mg/kg. The concentrations of 7b in plasma, brain, liver, kidney and muscle were measured by mass spectrometry at different time points (Fig. 3, Table 3). In plasma, the peak concentration of 7b was 68.29 ng/mL (156.28 nM) at 2.25 h after oral administration (Fig. 3a). In the brain (the target organ), the peak concentration of 7b was 4.02 ng/g (9.20 nmol/g) at 2.75 h (Fig. 3b). In the liver and kidney, the peak concentration of 7b was 148.40 ng/g (339.60 nmol/g) at 1.75 h (Figs. 3c) and 165.24 ng/g (378.14 nmol/g) at 2.50 h (Fig. 3d), respectively. Meanwhile, 7b was not detected in muscle (lower limit of detection: 0.6 ng/g) and is therefore unlikely to cause side-effects such as uncontrolled muscle contraction by inhibiting AChE at neuromuscular junctions. These results collectively demonstrate that 7b is absorbed *via* the gut and can penetrate the blood–brain barrier.

2.5. In vivo administration of 7b upregulates long-term potentiation

Proper hippocampal synaptic transmission is critical for learning and memory formation [27]. Such synaptic activity can be assessed by measuring electrophysiological responses in brain slices after stimulation [28,29]. Given that 7b can inhibit the AChE activity *in vitro* and penetrate the blood–brain barrier, its effects on synaptic activity were investigated by measuring LTP after electrical stimulation.

C57BL/6 mice were orally administered 7b (0.3, 1, or 3 mg/kg) or donepezil (0.7 mg/kg) daily for 4 days. Next, the neurons in the CA3 region of the hippocampus were stimulated by theta-burst stimulation, and the field excitatory postsynaptic potential (fEPSP) was measured in the CA1 region [30]. Brain slices obtained from 7b-treated mice (3 mg/kg) exhibit significant enhancement of LTP upon stimulation compared to vehicle-treated control mice, suggesting that 7b can enhance synaptic strength in the hippocampus (Fig. 4a and b).

Acetylcholine signals *via* muscarinic M1 receptor at the postsynaptic neurons in the hippocampus [31]. Meanwhile, M1 receptor regulates neurotransmission and synaptic plasticity in the hippocampal circuits responsible for the modulation of cognitive function [32]. M1 receptor activity decreases during aging and neurodegeneration, suggesting that its agonist is a potential therapeutic target for Alzheimer's disease [33,34]. Therefore, to investigate whether 7b benefits cholinergic transmission, its effect on LTP was examined in acute hippocampal brain slices treated with pirenzepine, a selective M1 muscarinic acetylcholine receptor

Table 3
Pharmacokinetics study of 7b

Dose	Tissue	$t_{1/2}$	T_{max}	C_{max}	$AUC_{(0-t)}$	$AUC_{(0-\infty)}$	$MRT_{(0-\infty)}$
		h	h	ng mL^{-1} or g^{-1}	ng mL^{-1} or g^{-1} · h	ng mL^{-1} or g^{-1} · h	h
7b (10 mg/kg)	Plasma	7.89	2.25	68.29	245.70	279.38	10.80
	Brain	7.80	2.75	4.02	14.50	21.86	11.09
	Liver	7.16	1.75	148.40	488.56	534.14	8.39
	Kidney	7.49	2.50	165.24	901.81	1124.93	11.12

$t_{1/2}$: Terminal phase half-life; C_{max}: maximum concentration observed; T_{max}: time at C_{max} observed; $AUC_{(0-t)}$: area under the concentration − time curve up to the last measurable concentration; $AUC_{(0-\infty)}$: AUC up to infinite time; $MRT_{(0-\infty)}$: time needed for 63.3% of the dose to be eliminated *via* all routes of elimination.

antagonist used to impair LTP [35]. Accordingly, brain slices were pretreated with 7b (1 μM) or saline (*i.e.*, vehicle control) for 90 min before stimulation. The brain slices were treated with pirenzepine (10 μM) 30 min before stimulation, which significantly decreased LTP compared to the saline-treated controls. Meanwhile, pretreatment with 7b significantly ameliorated the LTP impairment induced by pirenzepine (Fig. 5).

2.6. Transcriptomic analysis of 7b-treated mouse brains

To further understand the effects of 7b *in vivo*, transcriptomic analysis of RNA sequencing was performed on total RNA isolated from the hippocampi of mice orally administered 7b ($n = 4$, for each dose) and saline (vehicle control, $n = 5$). Among the 26535 genes detected in the hippocampal tissue, 13647 genes were obtained after filtering genes with low-expression (fragments per kilobase of exon model per million reads mapped [FPKM] >1). A total of 1683 genes was shown in volcano plot with raw $P < 0.05$ (Fig. 6a). Differential gene expression analysis (*i.e.*, DESeq2 with R package) was performed to reveal 7b-specific transcriptomic changes based on the gene count matrix [36]. A total of 33 genes were differentially regulated in the mouse hippocampi after 7b administration with an adjusted P value (P_{adj}) < 0.01 and absolute fold change (FC) > 1.5 (Table 4). The top regulated genes with FC > 2 were *Fos*, *Gatad2b*, *Npas4*, *Fosb*, *Arc*, *B3galnt2*, *Egr4* (upregulated), and *Gm31593*, *Znf707* with FC < −2 (downregulated) (Fig. 6a). Heatmap of the 33 differentially regulated genes was shown (Fig. 6b). Functional analysis of the differentially regulated genes was performed by Gene Ontology (GO) enrichment analysis. The results indicate that the differentially regulated genes are correlated with biological processes (top 3) including RNA polymerase II (GO:0045944, raw $P = 1.01 \times 10^{-5}$; *Fos*, *Fosb*, *Npas4, Egr4*, *Egr1*, *Nr4a1*, *Ier2, Znf639*, *Klf2*), long-term memory (GO:0007616, raw $P = 1.89 \times 10^{-5}$; *Arc*, *Egr1*, *Npas4*), regulation of p38 MAPK cascade (GO:1900744, raw $P = 2.03 \times 10^{-5}$; *Dusp1*, *Gadd45b*, *Gadd45g*) (Fig. 6c).

Surprisingly, the differentially regulated genes included in the top 3 pathways emerged a fleet of immediate early genes (IEGs) that playing consolidated roles in the regulation of synaptic plasticity and memory [37]. IEGs such as *Arc*, *Egr1*, and *Fos*, were significantly upregulated in the hippocampi of 7b-treated mice. For example, *Arc* and *Egr1* induction is critical for LTP formation and memory consolidation [38,39]; *Fos* is increased in astrocytes during neuronal potentiation and memory enhancement [40]. *Npas4* affects synapses in neurons and promotes plasticity and memory formation [41]. The results here suggested that 7b enhances the synaptic activity and may promote cognitive function, through the regulation of multiple IEGs' expression.

To corroborate the expression changes of the differentially regulated genes from RNA sequencing above, the expressions of some genes were validated in hippocampal tissues from 7b-treated mice by real-time PCR analysis (*i.e.*, TaqMan gene expression assay) (Fig. 6d). Accordingly, the expressions of *Arc*, *Egr1*, *Fos* and *Dusp1* were elevated in the hippocampal tissues of 7b-treated mice to extents comparable to those in the RNA sequencing data.

3. Conclusion

We used 6-chlorotacrine and a moiety of huperzine A to design and synthesize a series of heterodimeric compounds that are connected by a methylene linker. These heterodimers exhibit superior AChE inhibitory compared to tacrine. With its tri-methylene linker, 7b exhibits the highest potency and best toxicity ratio among the series. Meanwhile, 7b inhibits AChE with an IC_{50} several magnitudes smaller than that of tacrine. Furthermore, 7b exhibits

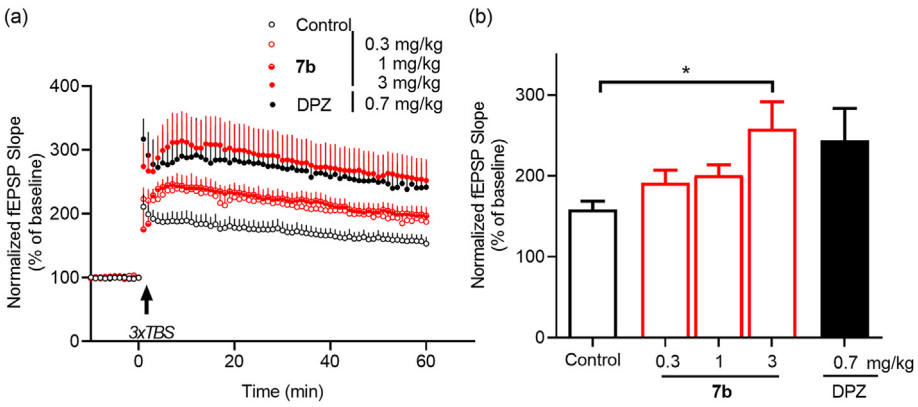

Fig. 4. Administration of 7b enhances long-term potentiation (LTP) in the mouse hippocampus. C57BL/6 mice were orally administered 7b or donepezil (DPZ) for 4 days. (a) The time-course of field excitatory postsynaptic potential (fEPSP) slope. Data are the averaged slopes of baseline-normalized fEPSP (mean ± SEM). LTP was induced by 3 × theta-burst stimulation (TBS), and traces recorded 30 min before and 60 min after stimulation are shown. (b) Quantification of mean fEPSP slopes in the last 10 min of recording after LTP induction (data are mean ± SEM; $n = 6$–10 slices from 4 to 5 brains per treatment). Mice treated with 7b exhibited a dose-dependent enhancement of LTP compared to vehicle-treated controls (*$P < 0.05$; ordinary one-way ANOVA followed by Tukey's multiple comparisons).

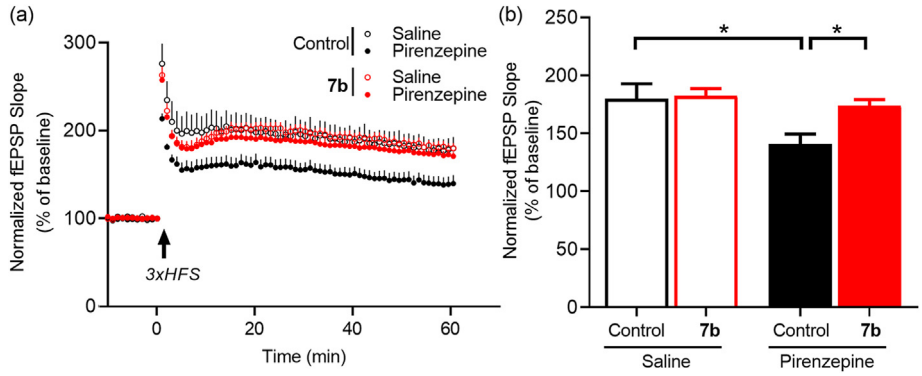

Fig. 5. Administration of 7b *in vitro* prevents the hippocampal long-term potentiation (LTP) impairment induced by pirenzepine. (a) Time-course of normalized field excitatory postsynaptic potential (fEPSP) slope. Data are the averaged slopes of baseline-normalized fEPSP (mean ± SEM). LTP was induced by 3 × high-frequency stimulation (HFS), and traces recorded 30 min before and 60 min after stimulation are shown. LTP induction was significantly impaired by pirenzepine (10 μM) but was attenuated by pretreatment with 7b (1 μM). (b) Quantification of mean fEPSP slopes in the last 10 min of recording after LTP induction (data are mean ± SEM; $n = 5–6$ slices from 3 brains per condition; $^*P < 0.05$; ordinary one-way ANOVA followed by Tukey's multiple comparisons).

preferential selectivity for AChE over BChE. The molecular docking study revealed a dual-binding property of 7b towards AChE that explains its high potency for AChE inhibition. In addition, the pilot pharmacokinetics study shows that 7b can enter the systemic blood circulation and the brain after oral administration. The *in vivo* electrophysiological study further shows that 7b administration enhances neurotransmission in the hippocampus in mice. Finally, transcriptomic analysis of hippocampal tissue from 7b-treated mice revealed the regulation of a group of IEGs, suggesting that 7b potentially affects pathways involved in memory formation. These results collectively suggest that 7b is a promising candidate for the development of a cognitive enhancer or therapy for dementias.

4. Experimental

4.1. General

Unless otherwise noted, starting materials and reagents were purchased from commercial sources and used without further purification. Air- or moisture-sensitive reactions were conducted in a nitrogen atmosphere. Anhydrous solvents were obtained from Sigma-Aldrich. Chromatography was performed using silica gel (60 Å pore diameter, 230–400 μm mesh size; Merck) using standard techniques. NMR spectra were recorded on either a Bruker 300 Ultra-Shield spectrometer at a [^{1}H] frequency of 300 MHz and a [^{13}C] frequency of 75 MHz or a Bruker 400 Ascend spectrometer at a [^{1}H] frequency of 400 MHz and a [^{13}C] frequency of 100 MHz. Chemical shifts (δ) are given in ppm relative to tetramethylsilane or the respective NMR solvent. Apparent peak multiplicities are described as *s* (singlet), *br s* (broad singlet), *d* (doublet), *dd* (doublet of doublets), *t* (triplet), *q* (quartet), or *m* (multiplet) where appropriate. Coupling constants (*J*) are reported in hertz after integration. All final compounds were ≥95% pure as determined by a Waters e2695 HPLC using reversed phase column (SunFire, C18 5 μm, 4.6 × 150 mm) and a solvent gradient of solvent A (H_2O with 0.01% TEA) and solvent B (CH_3CN): 0–15.0 min, B 30–85%; 15.0–23.0 min, B 85.0%; 23.0–25.0 min, B 85-30%. High-resolution ESI mass spectrum analysis was performed on a Waters Xevo G2-XS Q-TOF mass spectrometer. All spectral profiles are described in the *Supplementary Information S2*.

4.2. Chemistry

The 2 fragments that constitute the heterodimers (7a–7i)—1,5,7,8-tetrahydro-quinoline-2,6-dione (3) and *N*-(6-chloro-1,2,3,4-tetrahydroacridin-9-yl)-alkane-1,ω-diamine (6a–6i)—were obtained by two 2-step reactions as previously described [18–22]. The yields to obtain 3 from 1 and 6a–6i from 4 were 27.9% and 51.4–72.2%, respectively. Sodium triacetoxyborohydride (110 mg, 0.52 mmol) and a catalytic amount of acetic acid (8.5 μL) were added to a mixture of appropriate 6a–6i (50 mg, 0.17 mmol) and 3 (31 mg, 0.19 mmol) in dichloromethane (5 mL). After stirring at room temperature for 48 h, the reaction was quenched by adding saturated sodium bicarbonate (10 mL). The mixture was extracted with dichloromethane (10 mL × 3). The combined organic layer was dried over sodium sulfate, filtered and concentrated under reduced pressure, and purified by column chromatography on silica gel column with 10% methanol/1% ammonium hydroxide in dichloromethane, resulting in the desired product 7a–7i (yield: 34.0–43.0%).

4.2.1. 7a: 6-[(2-{(6-chloro-1,2,3,4-tetrahydroacridin-9-yl)amino}ethyl)amino]-5,6,7,8-tetrahydroquinolin-2(1H)-one

Compound 7a was prepared from 6a at 43% yield per the procedure described above. ^{1}H NMR (400 MHz, $CDCl_3$): δ 7.99–7.86 (m, 3H), 7.22–7.15 (m, 1H), 6.37 (d, $J = 9.2$ Hz, 1H), 3.60–3.52 (m, 2H), 3.09–2.87 (m, 12H), 1.91–1.82 (m, 4H). ^{13}C NMR (100 MHz, $CDCl_3$): δ 165.14, 159.58, 151.12, 148.01, 144.03, 142.45, 134.13, 127.48, 124.66, 124.35, 118.53, 117.34, 116.14, 112.49, 52.21, 48.81, 47.07, 34.00, 33.37, 27.79, 25.03, 24.76, 23.06, 22.80. ESI-HRMS (*m/z*) $[M+H]^+$: 423.1931 (calculated for $[C_{24}H_{28}ClN_4O]^+$: 423.1952).

4.2.2. 7b: 6-[3-(6-chloro-1,2,3,4-tetrahydro-acridin-9-ylamino)-propylamino]-5,6,7,8-tetrahydro-1H-quinolin-2-one

Compound 7b was prepared from 6b at 37% yield per the procedure described above. ^{1}H NMR (300 MHz, $CDCl_3$): δ 7.91 (d, $J = 9.1$ Hz, 1H), 7.84 (d, $J = 2.1$ Hz, 1H), 7.21 (dd, $J = 9.1$, 2.2 Hz, 1H), 7.17 (d, $J = 9.2$ Hz, 1H), 6.37 (d, $J = 9.1$ Hz, 1H), 5.19 (s, 1H), 3.67–3.57 (m, 2H), 2.98 (m, 2H), 2.89 (m, 2H), 2.84–2.71 (m, 3H), 2.60 (s, 2H), 2.31 (m, 1H), 2.09–1.95 (m, 1H), 1.95–1.74 (m, 8H), 1.74–1.59 (m, 1H). ^{13}C NMR (75 MHz, $CDCl_3$): δ 165.10, 159.57, 151.13, 148.33, 143.85, 142.50, 133.92, 127.60, 124.88, 124.00, 118.38, 117.25, 115.62, 112.46, 53.06, 49.24, 46.12, 34.14, 33.46, 31.64, 27.51, 25.25, 25.12, 23.10, 22.80. ESI-HRMS (*m/z*) $[M+H]^+$: 437.2110 (calculated for $[C_{25}H_{30}ClN_4O]^+$: 437.2108).

The bis-HCl salt of 7b was prepared by re-dissolving the solid in dichloromethane, and excess reagent HCl/Et_2O (1 M) was gradually added to the above solution while shaking the flask (~10 min) followed by concentration under reduced pressure to give 7b·2HCl as a yellow powder.

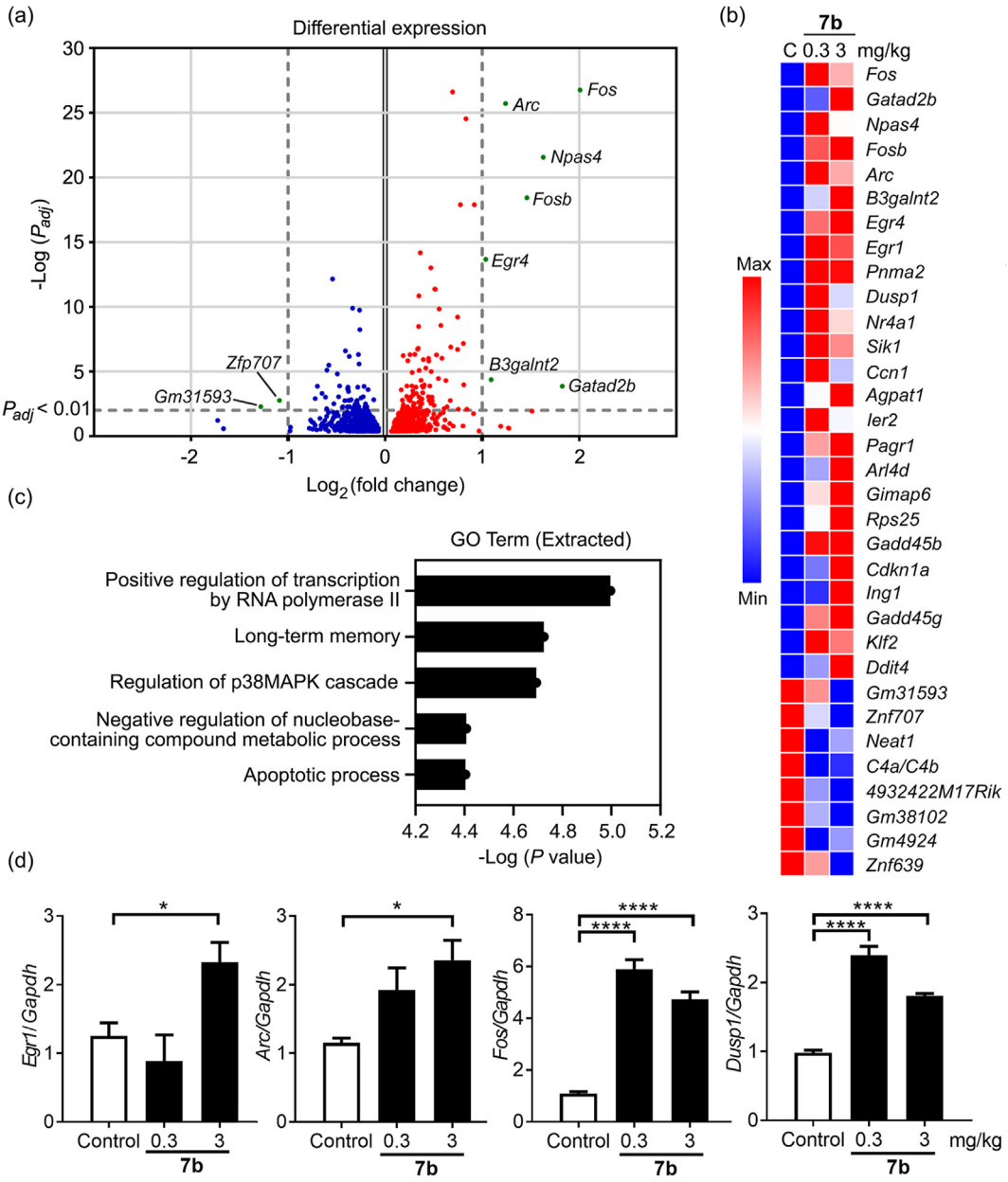

Fig. 6. Transcriptomic analysis of 7b-treated mouse hippocampi. (a) Differential expression of 7b-treated (3 mg/kg) versus control for all genes with FPKM >1 and raw $P < 0.05$. Dotted lines indicate $P_{adj} < 0.01$ and FC > 2 or < −2. Upregulated genes in 7b-treated hippocampi are in red, and genes that are downregulated are in blue. The top 9 up- and downregulated genes with FC > 2 or < −2 are labeled and in green. (b) Heatmap of 33 differentially regulated genes with FC > 1.5 or < −1.5 and $P_{adj} < 0.01$ in 7b-treated mice (3 mg/kg). (c) Gene Ontology (GO) enrichment analysis on 33 differentially regulated genes. Bar graph indicated the pathways (top 5) resulted from the analysis with corresponding −log (*P* value). (d) Quantitative real-time PCR analysis of *Egr1*, *Arc*, *Fos* and *Dusp1*. Vehicle (control), $n = 5$; 7b (0.3 mg/kg), $n = 4$; 7b (3 mg/kg), $n = 4$. All data are mean ± SEM (*$P < 0.05$, ****$P < 0.0001$; ordinary one-way ANOVA followed by Tukey's multiple comparisons).

4.2.3. 7c: 6-[(4-{(6-chloro-1,2,3,4-tetrahydroacridin-9-yl)amino} butyl)amino]-5,6,7,8-tetrahydroquinolin-2(1H)-one

Compound 7c was prepared from 6c at 40% yield per the procedure described above. ^{1}H NMR (300 MHz, $CDCl_3$) δ 7.91–7.82 (m, 2H), 7.29–7.21 (m, 1H), 7.16 (d, $J = 9.2$ Hz, 1H), 6.37 (d, $J = 9.1$ Hz, 1H), 4.74 (s, 2H), 4.02 (s, 1H), 3.48 (t, $J = 6.3$ Hz, 2H), 3.01 (s, 2H), 2.93–2.75 (m, 2H), 2.69 (m, 6H), 2.26 (m, 1H), 1.89 (m, 4H), 1.71 (m, 2H), 1.61–1.54 (m, 2H). ^{13}C NMR (75 MHz, $CDCl_3$) δ 165.06, 159.81, 150.86, 148.31, 144.00, 142.47, 134.14, 127.76, 124.65, 124.45, 118.63, 117.30, 116.14, 112.70, 52.91, 49.58, 46.92, 34.19, 33.48, 29.75, 28.01, 27.78, 25.41, 24.85, 23.08, 22.81. ESI-HRMS (*m/z*) $[M+H]^+$: 451.2268 (calculated for $[C_{26}H_{32}ClN_4O]^+$: 451.2265).

4.2.4. 7d: 6-[(5-{(6-chloro-1,2,3,4-tetrahydroacridin-9-yl)amino} pentyl)amino]-5,6,7,8-tetrahydroquinolin-2(1H)-one

Compound 7d was prepared from 6d at 37% yield per the procedure described above. ^{1}H NMR (300 MHz, $CDCl_3$) δ 7.87 (m, 2H), 7.25 (m, 1H), 7.22–7.09 (m, 1H), 6.37 (d, $J = 9.1$ Hz, 1H), 3.48 (t, $J = 7.2$ Hz, 2H), 3.01 (s, 2H), 2.88 (m, 1H), 2.75 (m, 2H), 2.66 (m, 4H), 2.27 (m, 1H), 2.06–1.86 (m, 6H), 1.72–1.61 (m, 2H), 1.54–1.40 (m, 4H). ^{13}C NMR (75 MHz, $CDCl_3$) δ 165.00, 159.78, 150.87, 148.37, 143.99, 142.44, 134.12, 127.83, 124.69, 124.43, 118.61, 117.34, 116.03, 112.68, 52.96, 49.67, 47.19, 34.26, 33.50, 31.88, 30.33, 27.79, 25.47, 24.93, 24.80, 23.12, 22.85. ESI-HRMS (*m/z*) $[M+H]^+$: 465.2424 (calculated for $[C_{27}H_{34}ClN_4O]^+$: 465.2421).

Table 4
List of genes that are significantly regulated in the hippocampi of 7b-treated mice. Fold change (FC) and adjusted *P* value (P_{adj}) were calculated using DESeq2 based on the normalized gene count matrix of 7b- (3 mg/kg) and vehicle (Con)-treated C57BL/6 mice. Differentially regulated genes with FC > 1.5 or < −1.5 and a $P_{adj} < 0.01$ were shown. Individual genes were presented in mean of fragments per kilobase of exon model per million reads mapped (FPKM) of the replicates of each group.

Gene	Fold Change	P_{adj}	FPKM	
			Con	7b
Fos	4.021	1.78E-27	3.27	13
Gatad2b	3.545	1.39E-04	4.698	9.648
Npas4	3.095	2.76E-22	1.073	3.335
Fosb	2.752	3.72E-19	2.068	5.431
Arc	2.363	1.92E-26	28.083	66.555
B3galnt2	2.133	4.29E-05	3.042	4.747
Egr4	2.052	2.13E-14	11.342	23.344
Egr1	1.891	1.29E-18	20.982	39.783
Pnma2	1.793	8.21E-03	2.957	4.812
Dusp1	1.789	2.86E-37	5.953	10.785
Nr4a1	1.782	2.97E-25	17.897	31.949
Sik1	1.754	1.07E-04	2.243	3.935
Ccn1	1.748	6.82E-08	1.519	2.666
Agpat1	1.718	1.55E-37	28.944	48.155
Ier2	1.713	1.29E-18	3.302	5.675
Pagr1	1.687	8.21E-03	1.934	3.103
Arl4d	1.678	6.20E-10	7.787	13.094
Gimap6	1.677	1.99E-07	1.811	2.972
Rps25	1.619	2.49E-27	62.259	96.137
Gadd45b	1.599	1.29E-07	9.059	14.416
Cdkn1a	1.593	1.77E-03	3.833	6.122
Ing1	1.557	5.32E-03	8.388	11.999
Gadd45g	1.544	5.04E-05	13.734	21.126
Klf2	1.524	7.39E-03	4.835	7.387
Ddit4	1.501	9.35E-07	33.255	49.931
Gm31593	−2.429	5.25E-03	3.17	1.538
Znf707	−2.127	1.72E-03	3.798	1.866
Neat1	−1.647	1.23E-03	5.602	3.662
C4a/C4b	−1.622	1.37E-04	10.192	6.153
4932422M17Rik	−1.569	4.99E-04	2.347	1.498
Gm38102	−1.531	9.70E-04	2.445	1.597
Gm4924	−1.519	7.54E-03	1.469	1.262
Znf639	−1.516	7.93E-06	12.376	7.802

4.2.5. 7e: 6-[(6-{(6-chloro-1,2,3,4-tetrahydroacridin-9-yl)amino} hexyl)amino]-5,6,7,8-tetrahydroquinolin-2(1H)-one

Compound 7e was prepared from 6e at 38% yield per the procedure described above. ^{1}H NMR (300 MHz, $CDCl_3$) δ 7.90−7.83 (m, 2H), 7.31−7.24 (m, 1H), 7.18 (d, J = 9.2 Hz, 1H), 6.37 (d, J = 9.3 Hz, 1H), 3.94 (m, 1H), 3.47 (m, 2H), 3.02 (s, 2H), 2.87 (m, 1H), 2.83−2.72 (m, 2H), 2.72−2.59 (m, 4H), 2.29 (m, 1H), 2.07−1.95 (m, 1H), 1.91 (m, 4H), 1.74−1.56 (m, 2H), 1.56−1.44 (m, 2H), 1.44−1.28 (m, 4H). ^{13}C NMR (75 MHz, $CDCl_3$) δ 165.14, 159.73, 150.88, 148.34, 143.96, 142.61, 134.03, 127.76, 124.71, 124.32, 118.57, 117.17, 115.93, 112.76, 52.95, 49.68, 47.24, 34.22, 33.50, 31.88, 30.48, 27.79, 27.29, 26.98, 25.42, 24.72, 23.07, 22.80. ESI-HRMS (m/z) $[M+H]^+$: 479.2579 (calculated for $[C_{28}H_{36}ClN_4O]^+$: 479.2578).

4.2.6. 7f: 6-[(7-{(6-chloro-1,2,3,4-tetrahydroacridin-9-yl)amino} heptyl)amino]-5,6,7,8-tetrahydroquinolin-2(1H)-one

Compound 7f was prepared from 6f at 37% yield per the procedure described above. ^{1}H NMR (300 MHz, $CDCl_3$) δ 7.95−7.85 (m, 2H), 7.31−7.24 (m, 1H), 7.19 (d, J = 9.2 Hz, 1H), 6.39 (d, J = 9.1 Hz, 1H), 3.95 (s, 1H), 3.47 (s, 2H), 3.03 (s, 2H), 2.89 (m, 1H), 2.83−2.73 (m, 2H), 2.71−2.64 (m, 4H), 2.30 (m, 1H), 2.06−1.87 (m, 6H), 1.64 (m, 4H); 1.49 (m, 2H), 1.35 (m, 6H). ^{13}C NMR (75 MHz, $CDCl_3$) δ 165.08, 159.74, 150.94, 148.37, 144.00, 142.56, 134.07, 127.79, 124.76, 124.34, 118.58, 117.23, 115.92, 112.78, 52.97, 49.77, 47.35, 34.25, 33.50, 31.91, 30.48, 29.44, 27.81, 27.47, 27.01, 25.48, 24.74, 23.11, 22.84. ESI-HRMS (m/z) $[M+H]^+$: 493.2732 (calculated for $[C_{29}H_{38}ClN_4O]^+$: 493.2734).

4.2.7. 7g: 6-[(8-{(6-chloro-1,2,3,4-tetrahydroacridin-9-yl)amino} octyl)amino]-5,6,7,8-tetrahydroquinolin-2(1H)-one

Compound 7g was prepared from 6g at 36% yield per the procedure described above. ^{1}H NMR (300 MHz, $CDCl_3$) δ 7.94−7.85 (m, 2H), 7.30−7.23 (m, 1H), 7.18 (d, J = 9.2 Hz, 1H), 6.38 (d, J = 9.1 Hz, 1H), 3.93 (s, 1H), 3.47 (d, J = 5.7 Hz, 2H), 3.08−2.97 (m, 2H), 2.77 (t, J = 5.8 Hz, 2H), 2.65 (m, 4H), 2.29 (m, 1H), 1.96 (m, 2H), 1.72−1.56 (m, 4H), 1.49 (m, 2H), 1.43−1.21 (m, 10H). ^{13}C NMR (75 MHz, $CDCl_3$) δ 165.04, 159.75, 150.95, 148.41, 143.99, 142.54, 134.06, 127.83, 124.77, 124.33, 118.60, 117.27, 115.91, 112.77, 52.99, 49.80, 47.43, 34.29, 33.55, 31.97, 30.57, 29.61, 29.44, 27.86, 27.48, 27.02, 25.52, 24.75, 23.12, 22.86. ESI-HRMS (m/z) $[M+H]^+$: 507.2885 (calculated for $[C_{30}H_{40}ClN_4O]^+$: 507.2891).

4.2.8. 7h: 6-[(9-{(6-chloro-1,2,3,4-tetrahydroacridin-9-yl)amino} nonyl)amino]-5,6,7,8-tetrahydroquinolin-2(1H)-one

Compound 7h was prepared from 6h at 35% yield per the procedure described above. ^{1}H NMR (300 MHz, $CDCl_3$) δ 7.93−7.82 (m, 2H), 7.27 (m, 1H), 7.18 (d, J = 9.2 Hz, 1H), 6.38 (d, J = 9.1 Hz, 1H), 3.94 (s, 1H), 3.48 (s, 2H), 3.02 (s, 2H), 2.89 (s, 1H), 2.70−2.63 (m, 6H), 2.30 (m, 1H), 1.96 (m, 2H), 1.68−1.62 (m, 2H), 1.45−1.51 (m, 2H), 1.23−1.41 (m, 14H). ^{13}C NMR (75 MHz, $CDCl_3$) δ 164.97, 159.76, 150.99, 148.42, 144.01, 142.46, 134.08, 127.83, 124.78, 124.34, 118.61, 117.34, 115.90, 112.78, 52.99, 49.82, 47.46, 34.28, 33.54, 31.97, 30.58, 29.61, 29.45, 27.88, 27.54, 27.06, 25.56, 24.75, 23.13, 22.86. ESI-HRMS (m/z) $[M+H]^+$: 521.3052 (calculated for $[C_{31}H_{42}ClN_4O]^+$: 521.3047).

4.2.9. 7i: 6-[(10-{(6-chloro-1,2,3,4-tetrahydroacridin-9-yl)amino} decyl)amino]-5,6,7,8-tetrahydroquinolin-2(1H)-one

Compound 7i was prepared from 6i at 34% yield per the procedure described above. ^{1}H NMR (300 MHz, $CDCl_3$) δ 7.96−7.81 (m, 2H), 7.31−7.22 (m, 1H), 7.18 (d, J = 9.2 Hz, 1H), 6.38 (d, J = 9.1 Hz, 1H), 3.95 (s, 1H), 3.47 (m, 2H), 3.02 (m, 2H), 2.89 (m, 1H), 2.78 (m, 2H), 2.70−2.62 (m, 5H), 2.30 (m, 1H), 2.05−1.93 (m, 2H), 1.65 (m, 3H), 1.48 (m, 2H), 1.30 (m, 14H). ^{13}C NMR (75 MHz, $CDCl_3$) δ 165.12, 159.69, 150.97, 148.35, 143.98, 142.61, 134.03, 127.73, 124.77, 124.27, 118.54, 117.17, 115.82, 112.84, 52.97, 49.78, 47.43, 34.22, 33.51, 31.94, 30.55, 29.65, 29.59, 29.45, 27.85, 27.54, 27.02, 25.50, 24.71, 23.08, 22.82. ESI-HRMS (m/z) $[M+H]^+$: 535.3204 (calculated for $[C_{32}H_{44}ClN_4O]^+$: 535.3204).

4.3. In vitro cholinesterase activity assay

The *in vitro* cholinesterase activity assay was conducted as previously described [42]. Sprague−Dawley rats were supplied by the Animal and Plant Care Facility of The Hong Kong University of Science and Technology (HKUST). The experimental protocols were approved by the Animal Ethics Committee of HKUST and conducted in accordance with the Code of Practice Care and Use of Animals for Experimental Purposes of Hong Kong. Briefly, cortices and sera collected from rats were used as sources of AChE and BChE, respectively. The traditional Ellman method modified to run in 96-well plates (NUNC) was used for this assay. The cholinesterase inhibitory activities of the compounds suppressed the breakdown of the substrate acetyl (or butyryl) thiocholine iodide (0.83 and 1.25 mM, respectively) to thiocholine, which then reacted with 5,5′-dithio-bis-(2-nitrobenzoic) acid (DTNB) to form the yellow 5-thio-2-nitro-benzoic acid that was detected at an absorbance of 405 nm.

The concentration−response curve of each compound was obtained, and the IC_{50} was determined using GraphPad Prism version 5. Each reaction was performed in duplicate, and IC_{50s} values are presented as the mean ± SEM of at least 3 independent

experiments. The inhibitory specificity of each compound was calculated as a ratio of its IC_{50} for BChE to its IC_{50} for AChE.

To study the inhibitory mechanism, AChE was mixed with thiocholine iodide (0.16–1 mM), DTNB (0.32 mM), and inhibitor (7b or tacrine) in a 50-μL reaction at 37 °C for 15 min in a spectrophotometer (VersaMax); A405 was measured continuously every 20 s. The average rate of the reaction during the initial 5 min was used to construct Lineweaver–Burk plots.

4.4. In vitro toxicity assay

The cardiotoxicity of compounds was assessed by measuring their inhibitory effect on the cardiac potassium channel hERG. The Chinese hamster ovary (CHO–K1) cell line stably expressing hERG was a kind gift of Dr. A.L. George (Northwestern University, Chicago, IL, USA) [43]. Cells were grown in HAMS F-12 media with L-glutamine supplemented with 10% FBS and 1% penicillin–streptomycin in a humidified, 5% CO_2 incubator at 37 °C. Cells were seeded on 96-well plates at 80% confluency and incubated overnight at 30 °C to increase cell membrane expression. Thallium ion was used as a surrogate for potassium ion, and thallium influx was measured using the FluxOR Potassium Ion Channel Assay kit (Invitrogen) according to the manufacturer's instructions. The cells were incubated with compounds for 30 min, and thallium influx was then measured by fluorescence using FLIPR Tetra (Molecular Devices). The baseline fluorescence was obtained in the presence of 100 μM cisapride, a potent inhibitor of hERG (with an IC_{50} of ~35 nM using this kit and the CHO hERG cells).

The liver toxicity of the compounds was assessed by measuring their cytotoxicity on human hepatoma HepG2 cells (American Type Culture Collection) [44]. HepG2 cells were maintained in DMEM supplemented with 10% heat-inactivated FBS and incubated at 37 °C. Cells were seeded on 96-well plates at 20,000 cells per well. The cells were then treated with serial concentrations of compound for 24 h. MTT was added to a final concentration of 0.5 mg/mL. The concentration of formazan, an indicator of the number of living cells, was measured by absorbance at 550 nm using a VersaMax tunable microplate reader (Molecular Devices).

4.5. In vivo pharmacokinetics study

The *in vivo* pharmacokinetics study was performed as previously described [45]. The procedures were approved by HKUST Animal Ethics Committee and conducted in accordance with the Code of Practice and Use of Animals for Experimental Purpose. Twelve-week-old C57BL/6 mice were orally administered a single dose of 7b at 10 mg/kg. The terminal blood samples (collected into tubes containing K_2EDTA) and brain tissues were obtained at 0, 0.25, 0.5, 1, 2, 3, 4, 8 and 24 h post-dose ($n = 4$ per time point). The blood samples were centrifuged at 3000 rpm for 15 min at 4 °C to separate the plasma. After a 30-min cardiac perfusion with 0.9% saline to thoroughly expel the blood, brain, liver and kidney tissues were collected and follow homogenized with 0.9% saline (0.1 mL). The plasma (150 μL), brain, liver and kidney homogenate, and blank samples were extracted with 1 mL methanol twice. The supernatants were combined and evaporated to dryness, and then 0.2 mL methanol was accurately added to dissolve and centrifuged. The supernatant (80 μL) was accurately transferred into vial for UPLC-MS/MS analysis. The quantity of 7b in the tissue samples was determined by UPLC coupled with triple-quadrupole mass spectrometry (Waters Acquity UPLC coupled to an AB SCIEX 4500 QTRAP system). Details of the detection parameters are provided in the *Supplementary Information S3*.

4.6. Electrophysiological recording of mouse brain slices

Twelve-week-old C57BL/6 mice were orally administered 7b (in salt form) at 0.3, 1, or 3 mg/kg or donepezil (0.7 mg/kg) daily for 4 days; before oral administration, both 7b and donepezil were freshly dissolved in water and administered at 10 mL/kg.

Briefly, the mice were sacrificed, and their brains were dissected and sectioned at 300 μm using a vibrating microtome (HM650V, Thermo Scientific). Hippocampal regions were isolated and placed on a MED–P210A probe fabricated with 8 × 8 electrode arrays (Panasonic International). The slices were recovered in ice-cold artificial cerebrospinal fluid in 95% O_2/5% CO_2 at 32 °C. An electrode placed in the Schaffer collateral pathway was used as the stimulating electrode, and fEPSPs were recorded from the dendritic layer of CA1 neurons. The stimulation intensity that evoked a fEPSP with 50% of the maximum response was applied. LTP was induced by 3 trains of theta-burst stimulation. LTP formation was recorded using a multielectrode array system (MED-64, Panasonic International), and paradigms were conducted as previously described [30]. The magnitude of LTP was quantified as the percentage change in the average slope of the fEPSP over 60 min after induction. For acute hippocampal slice recording, hippocampal slices from C57BL/6 mice were pretreated with 7b (1 μM) or vehicle (saline) for 90 min. Then, pirenzepine (10 μM) or vehicle (saline) was added to the pretreated slices 30 min before stimulation. LTP was subsequently induced by 3 trains of high-frequency stimulation (100 Hz for 1 s, 30 s apart).

4.7. Computational docking

The crystal structures of mouse AChE (PDB code: 5DTI) and human BChE in complex with tacrine (PDB code: 4BDS) were obtained from the Protein Data Bank. The 3D structure of 7b was constructed by Discovery Studio version 2.5 and prepared as protonated at both segments with both *R*- and *S*-isomers. All water molecules and ligands were deleted, and hydrogen atoms were added to amino acid residues using GOLD version 5.1. The resultant enzyme structure was used as input for docking in GOLD. All ligand flexibility options were set as "on," and search efficiency was set to 200%. For AChE docking, the binding site was manually chosen to cover the whole active site gorge. Residues Tyr337 and Trp286 were set as flexible. Moreover, 7b was constrained by hydrogen binding between the protonated hydrogen on the tacrine ring and the carbonyl oxygen on His447. For BChE docking, the binding site was defined as follows: $x = 37.1830$, $y = 113.6900$, $z = 38.7860$, and radius = 20.834 Å. Moreover, 7b was constrained by hydrogen binding between the protonated hydrogen on the tacrine ring and the carbonyl oxygen on His438. Each docked system was performed with 20 GA runs. The docking results were visualized, and the structures of ligand–AChE complexes were generated using Hermes version 1.5. Graphic manipulations were performed using PyMol version 4.2.0. After docking, all conformations were visually inspected; a representative conformation is shown in Fig. 2.

4.8. Transcriptomic analysis and qRT-PCR

Total RNA from treated mouse hippocampi was extracted using TRIzol (Invitrogen) and the RNeasy Mini Kit (Qiagen). The RNA concentration was quantified using a BioDrop μLITE microvolume spectrophotometer. RNA was then submitted to eukaryotic transcriptomic analysis (Novogene). Differential expression analysis was performed using DESeq2 in the R/Bioconductor package (version 3.11) as previously described [36]. Differentially regulated genes were selected on the basis of the fold change (FC > 1.5 or < −1.5) of the normalized gene count matrix of treated mice

compared to the control. Volcano plot was generated suing Graphpad Prism (version 8.4.3). Heatmaps were generated using Morpheus (Broad Institute; https://software.broadinstitute.org/morpheus/). GO enrichment analysis was performed using the PANTHER overrepresentation test powered by PANTHER (http://pantherdb.org/) (annotation version: GO database, released 2020-02-21). Equivalent amounts of RNA were reverse-transcribed using the PrimeScript RT-PCR Kit (TaKaRa). Reverse-transcribed cDNA was then subjected to TaqMan gene expression assay (Applied Biosystems). Assays were conducted in a total volume of 20 μL containing 2 μL cDNA. The mRNA expression values were normalized to that of *Gapdh*. The following TaqMan probes were used: *Gapdh* (Mm99999915_g1), *Arc* (Mm01204954_g1), *Egr1* (Mm00656724_m1), *Fos* (Mm00487425_m1) and *Dusp1* (Mm00457274_g1).

4.9. Statistical analysis

The researchers who performed the electrophysiology and pharmacokinetics studies were blinded to the mouse treatments. GraphPad Prism version 8.0 was used for all statistical analyses. The significance of differences was determined by ordinary one-way ANOVA followed by Tukey's multiple comparisons. The level of significance was set at $P < 0.05$.

Author contributions

F.C.F.I., G.F. contributed equally to this work; F.C.F.I., G.F., Y.H., N.Y.I. conceived and designed the experiments; F.Y., F.K., P.S., C.Y.L., K.C., F.X. performed the experiments; F.C.F.I., G.F., F.L., N.Y.I. analyzed the data; F.C.F.I., G.F., F.L., N.Y.I. wrote the manuscript.

All the authors read and approved the final manuscript.

Funding

This study was supported by the Research Grants Council of Hong Kong [the Theme-Based Research Scheme (T13-607/12R and C6027-19 GF)], the National Key R&D Program of China (2017YFE0190000 and 2018YFE0203600), the Areas of Excellence Scheme of the University Grants Committee (AoE/M-604/16), the Innovation and Technology Commission (ITCPD/17–9 and ITS/136/13FP), the Guangdong Provincial Key S&T Program (2018B030336001), the Guangdong Provincial Fund for Basic and Applied Basic Research (2019B1515130004), the Shenzhen Knowledge Innovation Program (JCYJ20180507183642005 and JCYJ20170413173717055) to N.Y.I.

Notes

The authors declare no competing financial interest.

Declaration of competing interest

The authors declare that they have no known competing financial interests or personal relationships that could have appeared to influence the work reported in this paper.

Acknowledgments

The authors would like to thank Dr. Ka-Kit Yeung, and Prof. Kit-Yu Fu for their helpful discussion; and technical assistance of Mr. Ka Chun Lok and Mr. Wenbo Lyu in this work.

Appendix A. Supplementary data

Supplementary data to this article can be found online at https://doi.org/10.1016/j.ejmech.2021.113827.

References

[1] M.G. Blake, M.M. Boccia, Basal forebrain cholinergic system and memory, Curr. Top. Behav. Neurosci. 37 (2018) 253–273, https://doi.org/10.1007/7854_2016_467.
[2] P. Schneider, H. Hampel, K. Buerger, Biological marker candidates of alzheimer's disease in blood, plasma, and serum, CNS Neurosci. Ther. 15 (2009) 358–374, https://doi.org/10.1111/j.1755-5949.2009.00104.x.
[3] R. Schliebs, T. Arendt, The cholinergic system in aging and neuronal degeneration, Behav. Brain Res. 221 (2011) 555–563, https://doi.org/10.1016/j.bbr.2010.11.058.
[4] F. Mangialasche, A. Solomon, B. Winblad, P. Mecocci, M. Kivipelto, Alzheimer's disease: clinical trials and drug development, Lancet Neurol. 9 (2010) 702–716, https://doi.org/10.1016/S1474-4422(10)70119-8.
[5] D.S. Raghuvanshi, N. Verma, S. Singh, S. Luqman, A. Chand Gupta, D.U. Bawankule, S. Tandon, A. Nagar, Y. Kumar, F. Khan, Design and synthesis of novel oleanolic acid based chromenes as anti-proliferative and anti-inflammatory agents, New J. Chem. 42 (2018) 16782–16794, https://doi.org/10.1039/c8nj03564d.
[6] N. Kandiah, M.C. Pai, V. Senanarong, I. Looi, E. Ampil, K.W. Park, A.K. Karanam, S. Christopher, Rivastigmine: the advantages of dual inhibition of acetylcholinesterase and butyrylcholinesterase and its role in subcortical vascular dementia and Parkinson's disease dementia, Clin. Interv. Aging 12 (2017) 697–707, https://doi.org/10.2147/CIA.S129145.
[7] H. Wang, H. Zhang, Reconsideration of anticholinesterase therapeutic strategies against alzheimer's disease, ACS Chem. Neurosci. 10 (2019) 852–862, https://doi.org/10.1021/acschemneuro.8b00391.
[8] M. Saxena, R. Dubey, Target enzyme in alzheimer's disease: acetylcholinesterase inhibitors, Curr. Top. Med. Chem. 19 (2019) 264–275, https://doi.org/10.2174/1568026619666190128125912.
[9] P. Sharma, M.K. Tripathi, S.K. Shrivastava, Cholinesterase as a target for drug development in alzheimer's disease, Methods Mol. Biol. 2089 (2020) 257–286, https://doi.org/10.1007/978-1-0716-0163-1_18.
[10] H. Dvir, I. Silman, M. Harel, T.L. Rosenberry, J.L. Sussman, Acetylcholinesterase: from 3D structure to function, Chem. Biol. Interact. 187 (2010) 10–22, https://doi.org/10.1016/j.cbi.2010.01.042.
[11] J.L. Sussman, M. Harel, I. Silman, Three-dimensional structure of acetylcholinesterase and of its complexes with anticholinesterase drugs, Chem. Biol. Interact. 87 (1993) 187–197, https://doi.org/10.1016/0009-2797(93)90042-W.
[12] A.K. Saxena, The structural hybrids of acetylcholinesterase inhibitors in the treatment of alzheimer's disease: a review, Alzheimer's Neurodegener. Dis. 4 (2019) 1–25, https://doi.org/10.24966/and-9608/100015.
[13] B. Svobodova, E. Mezeiova, V. Hepnarova, M. Hrabinova, L. Muckova, T. Kobrlova, D. Jun, O. Soukup, M.L. Jimeno, J. Marco-Contelles, J. Korabecny, Exploring structure-activity relationship in tacrine-squaramide derivatives as potent cholinesterase inhibitors, Biomolecules 9 (2019) 379, https://doi.org/10.3390/biom9080379.
[14] R. Xie, X. Mei, J. Ning, Design, synthesis and insecticide activity of novel acetylcholinesterase inhibitors: triazolinone and phthalimide heterodimers, Chem. Pharm. Bull. (Tokyo) 67 (2019) 345–350, https://doi.org/10.1248/cpb.c18-00704.
[15] J.M. Roldán-Peña, D. Alejandre-Ramos, Ó. López, I. Maya, I. Lagunes, J.M. Padrón, L.E. Peña-Altamira, M. Bartolini, B. Monti, M.L. Bolognesi, J.G. Fernández-Bolaños, New tacrine dimers with antioxidant linkers as dual drugs: anti-Alzheimer's and antiproliferative agents, Eur. J. Med. Chem. 138 (2017) 761–773, https://doi.org/10.1016/j.ejmech.2017.06.048.
[16] L. Pisani, M. Catto, A. De Palma, R. Farina, S. Cellamare, C.D. Altomare, Discovery of potent dual binding site acetylcholinesterase inhibitors *via* homo- and heterodimerization of coumarin-based moieties, ChemMedChem 12 (2017) 1349–1358, https://doi.org/10.1002/cmdc.201700282.
[17] M. Singh, M. Kaur, N. Chadha, O. Silakari, Hybrids: a new paradigm to treat Alzheimer's disease, Mol. Divers. 20 (2016) 271–297, https://doi.org/10.1007/s11030-015-9628-9.
[18] C.F. Lin, C.W. Chien, I. Ojima, Enantioselective Pd-catalyzed tandem allylic alkylation reaction using monodentate phosphoramidite ligands for the formal total synthesis of huperzine A, Org. Chem. Front. 1 (2014) 1062–1066, https://doi.org/10.1039/c4qo00180j.
[19] W.E. Bauta, W.R. Cantrell Jr., M.W. Tidwell, Reactivators of Organophosphorous Inhibited Acetylcholinesterase, Patent, 2014. US9162983B2.
[20] A. Hiremathad, R.S. Keri, A.R. Esteves, S.M. Cardoso, S. Chaves, M.A. Santos, Novel Tacrine-Hydroxyphenylbenzimidazole hybrids as potential multitarget drug candidates for Alzheimer's disease, Eur. J. Med. Chem. 148 (2018) 255–267, https://doi.org/10.1016/j.ejmech.2018.02.023.
[21] T.J. Eckroat, K.D. Green, R.A. Reed, J.J. Bornstein, S. Garneau-Tsodikova, Investigation of the role of linker moieties in bifunctional tacrine hybrids, Bioorg. Med. Chem. 21 (2013) 3614–3623, https://doi.org/10.1016/j.bmc.2013.02.047.

[22] J.J. Bornstein, T.J. Eckroat, J.L. Houghton, C.K. Jones, K.D. Green, S. Garneau-Tsodikova, Tacrine-mefenamic acid hybrids for inhibition of acetylcholinesterase, Medchemcomm 2 (2011) 406–412, https://doi.org/10.1039/c0md00256a.
[23] S. Diamant, E. Podoly, A. Friedler, H. Ligumsky, O. Livnah, H. Soreq, Butyrylcholinesterase attenuates amyloid fibril formation *in vitro*, Proc. Natl. Acad. Sci. U.S.A. 103 (2006) 8628–8633, https://doi.org/10.1073/pnas.0602922103.
[24] A. Alvarez, R. Alarcón, C. Opazo, E.O. Campos, F.J. Muñoz, F.H. Calderón, F. Dajas, M.K. Gentry, B.P. Doctor, F.G. De Mello, N.C. Inestrosa, Stable complexes involving acetylcholinesterase and amyloid-β peptide change the biochemical properties of the enzyme and increase the neurotoxicity of Alzheimer's fibrils, J. Neurosci. 18 (1998) 3213–3223, https://doi.org/10.1523/jneurosci.18-09-03213.1998.
[25] S. Qian, L. He, M. Mak, Y. Han, C.-Y. Ho, Z. Zuo, Synthesis, biological activity, and biopharmaceutical characterization of tacrine dimers as acetylcholinesterase inhibitors, Int. J. Pharm. 477 (2014) 442–453, https://doi.org/10.1016/j.ijpharm.2014.10.058.
[26] J. Cheung, M.J. Rudolph, F. Burshteyn, M.S. Cassidy, E.N. Gary, J. Love, M.C. Franklin, J.J. Height, Structures of human acetylcholinesterase in complex with pharmacologically important ligands, J. Med. Chem. 55 (2012) 10282–10286, https://doi.org/10.1021/jm300871x.
[27] J. Lisman, K. Cooper, M. Sehgal, A.J. Silva, Memory formation depends on both synapse-specific modifications of synaptic strength and cell-specific increases in excitability, Nat. Neurosci. 21 (2018) 309–314, https://doi.org/10.1038/s41593-018-0076-6.
[28] T.V.P. Bliss, G.L. Collingridge, A synaptic model of memory: long-term potentiation in the hippocampus, Nature 361 (1993) 31–39, https://doi.org/10.1038/361031a0.
[29] J.R. Whitlock, A.J. Heynen, M.G. Shuler, M.F. Bear, Learning induces long-term potentiation in the hippocampus, Science 313 (2006) 1093–1097, https://doi.org/10.1126/science.1128134.
[30] F.C. Ip, W.Y. Fu, E.Y. Cheng, E.P. Tong, K.C. Lok, Y. Liang, W.C. Ye, N.Y. Ip, Anemoside A3 enhances cognition through the regulation of synaptic function and neuroprotection, Neuropsychopharmacology 40 (2015) 1877–1887, https://doi.org/10.1038/npp.2015.37.
[31] L. Luo, W.H. Chen, M. Wang, D.M. Zhu, J.Q. She, D.Y. Ruan, Modulation of long-term potentiation by individual subtypes of muscarinic acetylcholine receptor in the rat dentate gyrus, Hippocampus 18 (2008) 989–995, https://doi.org/10.1002/hipo.20461.
[32] D. Fernández de Sevilla, A. Núñez, W. Buño, Muscarinic receptors, from synaptic plasticity to its role in network activity, Neuroscience S0306–4522 (2020) 30220–30227, https://doi.org/10.1016/j.neuroscience.2020.04.005.
[33] M. Scarpa, S. Hesse, S.J. Bradley, M1 muscarinic acetylcholine receptors: a therapeutic strategy for symptomatic and disease-modifying effects in Alzheimer's disease? Adv. Pharmacol. 88 (2020) 277–310, https://doi.org/10.1016/bs.apha.2019.12.003.
[34] B.J. Melancon, J.C. Tarr, J.D. Panarese, M.R. Wood, C.W. Lindsley, Allosteric modulation of the M1 muscarinic acetylcholine receptor: improving cognition and a potential treatment for schizophrenia and Alzheimer's disease, Drug Discov. Today 18 (2013) 1185–1199, https://doi.org/10.1016/j.drudis.2013.09.005.
[35] T. Masuoka, J. Uwada, M. Kudo, H. Yoshiki, Y. Yamashita, T. Taniguchi, M. Nishio, T. Ishibashi, I. Muramatsu, Augmentation of endogenous acetylcholine uptake and cholinergic facilitation of hippocampal long-term potentiation by acetylcholinesterase inhibition, Neuroscience 404 (2019) 39–47, https://doi.org/10.1016/j.neuroscience.2019.01.042.
[36] M.I. Love, W. Huber, S. Anders, Moderated estimation of fold change and dispersion for RNA-seq data with DESeq2, Genome Biol. 15 (2014) 550, https://doi.org/10.1186/s13059-014-0550-8.
[37] K. Minatohara, M. Akiyoshi, H. Okuno, Role of immediate-early genes in synaptic plasticity and neuronal ensembles underlying the memory trace, Front. Mol. Neurosci. 8 (2016) 78, https://doi.org/10.3389/fnmol.2015.00078.
[38] C.L. Peebles, J. Yoo, M.T. Thwin, J.J. Palop, J.L. Noebels, S. Finkbeiner, Arc regulates spine morphology and maintains network stability *in vivo*, Proc. Natl. Acad. Sci. U.S.A. 107 (2010) 18173–18178, https://doi.org/10.1073/pnas.1006546107.
[39] M.W. Jones, M.L. Errington, P.J. French, A. Fine, T.V.P. Bliss, S. Garel, P. Charnay, B. Bozon, S. Laroche, S. Davis, A requirement for the immediate early gene Zif268 in the expression of late LTP and long-term memories, Nat. Neurosci. 4 (2001) 289–296, https://doi.org/10.1038/85138.
[40] A. Adamsky, A. Kol, T. Kreisel, A. Doron, N. Ozeri-Engelhard, T. Melcer, R. Refaeli, H. Horn, L. Regev, M. Groysman, M. London, I. Goshen, Astrocytic activation generates de novo neuronal potentiation and memory enhancement, Cell 174 (2018) 59–71, https://doi.org/10.1016/j.cell.2018.05.002, e14.
[41] X. Sun, Y. Lin, Npas4: linking neuronal activity to memory, Trends Neurosci. 39 (2016) 264–275, https://doi.org/10.1016/j.tins.2016.02.003.
[42] Y. Hu, J. Zhang, O. Chandrashankra, F.C.F. Ip, N.Y. Ip, Design, synthesis and evaluation of novel heterodimers of donepezil and huperzine fragments as acetylcholinesterase inhibitors, Bioorg. Med. Chem. 21 (2013) 676–683, https://doi.org/10.1016/j.bmc.2012.11.044.
[43] F.M. Mullins, S.Z. Stepanovic, R.R. Desai, A.L. George, J.R. Balser, Extracellular sodium interacts with the HERG channel at an outer pore site, J. Gen. Physiol. 120 (2002) 517–537, https://doi.org/10.1085/jgp.20028589.
[44] Y.P. Ng, Y. Chen, Y. Hu, F.C.F. Ip, N.Y. Ip, Olean-12-eno[2,3-c] [1,2,5]oxadiazol-28-oic acid (OEOA) induces G1 cell cycle arrest and differentiation in human leukemia cell lines, PloS One 8 (2013), e63580, https://doi.org/10.1371/journal.pone.0063580.
[45] W. Luo, F.C.F. Ip, G. Fu, K. Cheung, Y. Tian, Y. Hu, A. Sinha, E.Y.L. Cheng, X. Wu, V. Bustos, P. Greengard, Y.M. Li, S.C. Sinha, N.Y. Ip, A pentacyclic triterpene from ligustrum lucidum targets γ-secretase, ACS Chem. Neurosci. 11 (2020) 2827–2835, https://doi.org/10.1021/acschemneuro.0c00389.